Accurate 3D location of mine induced seismicity in complex near-field underground conditions

Stella Coccia, Armand Lizeur, Pascal Bigarre, Isabelle Contrucci, Emmanuelle Klein

ACCURATE 3D LOCATION OF MINE INDUCED SEISMICITY IN COMPLEX NEAR-FIELD UNDERGROUND CONDITIONS

S. Coccia, A. Lizeur, P. Bigarré, I. Contrucci, E. Klein
INERIS, Nancy, France

Installation of local high resolution microseismic networks in the vicinity of hazardous mining fronts, and completing a pre-existing mine scale seismic network, is supposed to help detecting much smaller events and processing seismic data with much better accuracy, then gaining insight in the quantification of the rock mass response versus time, space and mine production, all critical parameters for rating the seismic hazard on a continuous basis.

However, the detection and processing of small magnitude events require some precautions due to near-field conditions adverse to the detection of significant changes in the seismic pattern. High resolution monitoring raises new issues related to the magnified complexity of the rock mass when dealing with higher frequency seismic waves travelling through the host rock, intersected by faults and geological disturbances, adjacent backfilled works intertwined with multilevel fast advancing mining works. This magnified complexity may introduce artefacts in the accurate location of the small magnitude sources, blurring the interpretation of the seismicity.

To face such situations of complex mining underground conditions, the authors intend to develop a new approach based on the implementation of 3D dynamic velocity model enabling to take into account not only the geological features surrounding a mining block, but the dynamic mining process itself, i.e. the creation of mining voids and surrounding disturbed zones.

Besides synthetic numerical tests that have been run to assess the relevance of this issue, the research work is tested through the back analysis of an intense microseismic swarm recorded during the brutal caving process of a solution mined cavern. This paper presents this numerical procedure currently being developed for operational implementation in the near future in deep mining works within the strategy of deployments of mobile local acoustic/microseismic arrays.

INTRODUCTION

Nowadays, the increasing need of ore extraction leads to the use of massive underground mining systems, such as cut-and-fill, sublevel and longhole stoping (artificially supported) or block and panel caving (naturally supported). They are highly productive mining methods, where ground stability issues can be severe and difficult to control for mining operators. For instance, block and panel caving miners have virtually no visual access to the cave and limited opportunities to install geotechnical instrumentation in the working area. In terms of risk mitigation this situation has been improved with the introduction of high resolution seismic system surrounding closely an area of interest (Handley[2006]).

Since its inception in the 1970s and its fast development from 1990's, seismic monitoring has proved to be invaluable tool for identifying underground areas at risk. However, the traditional mine-scale monitoring with its wide sensor spacing allows neither the recording of small events, nor the precise location of larger ones, limiting strongly the insight of any local seismogenic zone, where the stress gradient ahead of the mining front is breaking the rock (Potvin and Hudyma[2001]).

In addition, in the last decade, the mining production in underground hardrock mines has been also pushed to deeper levels, where the in situ and mine induced stresses are getting higher. This gives emphasis to the increasing necessity to ensure the safety of mine workers and minimize production losses by reinforcing the identification of rockburst potential areas.

To manage this seismic risk different engineering approaches have been proposed (Hudyma and Potvin[2010]), all based on analysis techniques of high resolution microseismic data.

It is well known that high resolution seismic monitoring can provide great benefits, but improving microseismic monitoring efficiency and accuracy at a mine requires a particular attention and sophisticated studies. With the installation of the microseismic monitoring system, a large amount of data was collected and it provides a unique opportunity for real time characterizations of fracture/failure processes in terms of event location, magnitude and source mechanisms (Iannacchione *et al.*[2003]).

Advances in seismic instrumentations have to correspond in advances in techniques of mining-induced seismicity. Without forget that every mine has its own specificity, generating particular type of ground motion, depending on the type of ore, technology and local geology (Zembaty[2004]).

A good understanding of mine induced seismicity relies strongly on the detection and correct location of all events in order to quantify the rock mass response to both the mining process and the geological mapped structures in the vicinity. Considering the complexity of the rock mass

response, seismic hazard may be rated for a mining block as an averaged index over a given time window but still considered to vary rapidly if not brutally, due to heterogeneity of the host rock, presence of highly stressed zones, goaf generation (that part of a mine from which the mineral has been partially or wholly removed; the waste left in old workings; – called also gob), etc., requiring to monitor the most complete induced seismicity catalogue. However, most mine-scale seismic networks are deployed at a much larger scale compared to a single mining work and have then the severe drawback of not detecting the numerous small magnitude microseismic events. This drawback can be managed in some specific situations by deploying locally a high resolution array, completing the coverage and resolution needed for any specific local mining work rated at risk. This may be seen as a temporary array set up and moving along with the mining.

The use of such mobile monitoring systems, aims first to complete largely the seismic catalogue for the area of interest and second to increase drastically the correctness of the calculated position of the high magnitude events, enhancing then significantly the ability to the mining staff to detect any significant change in the seismic activity versus the local geology encountered and the production rate. Concerning the latter, the correct location of any seismic event is critically important because not only a good location provides a guide for a rescue effort and other emergency plan, but all subsequent seismological processing relies on the event position. Eventually, any rockburst mitigation strategy originates from the correct 3D mapping of the seismic sources relatively to all the old or active mining works present in the area at risk. Source location uncertainties too large compared to the different emissive components of the monitored area affect obviously the capabilities to detect those changes ground engineers or mine seismologist are looking for.

It is well known that source location accuracy is affected by many factors. The most important ones are: sensor spatial distribution, accuracy in picking arrival times of seismic phases, knowledge of the velocity model, the computing of ray paths along with the location algorithm. For the mine environment, there are also other practical factors which play a fundamental role, such as mine layout, geology and various ground control issues.

The focus of this paper is to describe a new accurate microseismic event location approach to be used with high resolution monitoring systems in situations in which an evolving 3D velocity model is supposed of importance.

This works is being carried out thanks to the I2Mine (Innovative Technologies and Concepts for the Intelligent Deep Mine of the Future) FP7 European project, which focuses on the development of innovative technologies suitable for deep mining activities. It targets more especially health and safety issues, questions related to the working environment and the environmental implications and impacts.

LOCALISATION PARAMETERS

Data used to constrain event locations are usually derived from seismograms recorded at seismic stations, distributed around the monitored area and include arrival times and polarization angles.

Once the data quality is checked and phases are correctly picked the largest influence on the location of seismic events is related to the use of an advanced source location algorithm and the accuracy of the velocity model used for the rock mass. Thus, we have decided to deal with these aspects and their characteristics are discussed in the next sections.

LOCALISATION ALGORITHM

There are two broad groups of event location methods, namely "absolute location" and "relative location" methods. Absolute location is determined or specified within a fixed, geographic coordinate system and a fixed time base (e.g., Coordinated Universal Time, UTC). A relative location uses some or all of the seismograms from two or more neighbouring seismic events to locate them relatively to each other (Spence[1980] and Pavlis[1992]). This location is old and highly popular method, above all because the travel time anomalies resulting from velocity model uncertainties are removed implicitly. However, improvements in relative location accuracy obtained using the double-difference algorithm (Waldhauser and Ellsworth[2000, 2002]) and source specific station terms (Richards-Dinger and Shearer[2000]) often produce a dramatic sharpening of seismicity patterns, particularly when more accurate timing is obtained using waveform cross correlation (Shearer[2002]). Evaluating the performance of these methods is complicated, by the fact that the true earthquake locations are unknown.

Usually, an earthquake location is determined by an inverse problem: the match or misfit between observed arrival times of seismic wave-energy at seismic stations, and predictions of these arrival times for different source locations using a given elastic-wave speed model (Tarantola and Valette[1982]).

The general probabilistic solution to the inverse problem of event location from the available data is given by:

$$Q(\mathbf{m}) = k \cdot p(\mathbf{m}) \int_D \frac{p(\mathbf{d}) F(\mathbf{d}, \mathbf{m})}{\mu(\mathbf{d}, \mathbf{m})} d\mathbf{d}, \qquad (1)$$

where $\mathbf{m}$ denotes the vector of source location parameters (spatial coordinates and origin time) which takes values from parameter space $\mathbf{M}$; $p(\mathbf{m})$ is the prior *pdf* (probability density function) representing all information available about the location before (prior to) using the data

$\mathbf{d_{obs}}$ (e.g., arrival times); $p(\mathbf{d})$ is the *pdf* over a data space $\mathbf{D}$ describing the data uncertainty in $\mathbf{d_{obs}}$ due to measurement and processing uncertainties and $F(\mathbf{d},\mathbf{m})$ is the ability of the forward problem (e.g., travel time calculation) to predict the observed data (e.g., arrival times). The constant k normalizes Q to unit integral over $\mathbf{D}\times\mathbf{M}$ and $\mu(\mathbf{d},\mathbf{m})$ is the homogeneous distribution over data $\mathbf{d}$ and parameters $\mathbf{m}$.

It is usual to call the integral in (1) the *likelihood function* $L(\mathbf{m})$, which gives a (non-normalized) measure of how good any model $\mathbf{m}$ is in explaining the observed data $p(\mathbf{d})$.

With some simplifications (Lomax *et al.*[2009]) a maximum likelihood origin time, t_0, can be determined analytically from weighted means of the observed arrival times and the predicted travel times (e.g., Tarantola and Valette[1982]), and if the observed and predicted times are uncorrelated the likelihood function is:

$$L(\mathbf{x}) = \exp\left\{-\frac{1}{2}\sum_i \frac{\left[T_i^o - T_i^c(\mathbf{x})\right]^2}{\sigma_i^2}\right\}, \qquad (2)$$

where $\mathbf{x}$ is the spatial part of $\mathbf{m}$, T_i^o are observed travel times, T_i^c are the calculated travel times for observation i (i.e., T_i^c represents the travel time, rather than arrival time, part of $f(\mathbf{m})$), and σ_i summarizes the associated standard deviation of uncertainty in T_i^o and T_i^c.

Though not normalized, $L(\mathbf{x})$ is sufficient to provide the relative probability of any location $\mathbf{m}$ being the best estimate of the event location given the available data measurements. Since in practice integrating over all of $\mathbf{D}\times\mathbf{M}$ to find normalizing constant k in Equation 1 is often computationally intractable, the product of the prior, spatial location information $p(\mathbf{x})$ (i.e., the spatial part of $p(\mathbf{m})$) and the non-normalized likelihood $L(\mathbf{x})$ is usually taken as the objective function for inversion and searching in direct search location algorithms. If $L(\mathbf{x})$ is determined throughout the prior *pdf* $p(\mathbf{x})$ through a global-search, then Equation 1 can be normalized approximately after location. Therefore, according to Lomax *et al.*[2005, 2009] we refer to such an approximately normalized function, $p(\mathbf{x})L(\mathbf{x})$, as a location *pdf*.

Moreover, to solve the inverse problem for seismic source location we used the same procedure described by Lomax *et al.*[2009] and we focused on the Non-Linearized or Direct-Search methods.

Contrary to Linearized methods, the use of a Direct-Search location is easily applicable to realistic earth models, which may show abrupt and complicated velocity variations in three-dimensions. In addition, it imposes little restriction on the form of the measure of misfit, it is stable even with poorly constrained spatial locations or origin times, and it produces comprehensive, probabilistic solutions mapping the full location uncertainty, often a complex time-space function (Lomax *et al.*[2009]).

This non linear probabilistic location technique has widely been used for regional hypocenter location in highly heterogeneous areas (Lomax *et al.*[2001, 2005], Zollo *et al.*[2002], Husen *et al.*[2003], Presti *et al.*[2004] and Lippitsch *et al.*[2005]), and it has been also incorporated in more local micro-earthquake studies (Spillmann *et al.*[2007]).

We carried out all event locations with probabilistic absolute location using the Oct-Tree sampling algorithm to perform a global search within a parameter space $\mathbf{M}$. This algorithm can be easily applied with 3D velocity models because it does not require partial derivate information, which is difficult or impossible to obtain in complex models (Lomax *et al.*[2001]). It also permits a systematic coverage of search region and an accurate recovery of complex *pdf* (Lomax *et al.*[2009]).

Thus, in our study the hypocenter with the maximum likelihood is determined by using the Oct-Tree nonlinear method, which consists on a recursive subdivision and sampling of rectangular cells in three-dimensional space to generate a cascade structure of sampled cells, such that the spatial density of sampled cells follows the targeted *pdf* values. The relative probability that a seismic source location lies within any given cell i is approximately:

$$P_i = V_i\, L(\mathbf{x_i}), \qquad (3)$$

where V_i is the cell volume and $\mathbf{x_i}$ is the vector of coordinates of the cell center (Lomax *et al.*[2009]).

The likelihood function in Equation 1 is entirely defined by the probabilistic error processes involved. Sometimes it is desirable to change the approximations employed in Equation 2 in order to remove biases or instability in solution. Oct-tree sampling can use the L2-norm misfit function or the EDT (equal differential-time) formulation (Lomax[2005]) to represent the *pdf* of the data error variation, since both require searching over three-dimensional spatial locations only.

We noted that for our studies the L2-norm seems most appropriate to the area dimension respect to the EDT-norm, which fits well natural earthquake location and large-scale seismic networks. The L2-norm is preferred and in this case the location likelihood function is:

$$pdf_{LSL2} = k\exp\left\{-\sum_{obs_i}\frac{\left[T_{obs_i}(\mathbf{x}) - T_{calc_i}(\mathbf{x})\right]^2}{\sigma_i^2} - \sum_{obs_j}\frac{\left[\theta_{obs_j}(\mathbf{x}) - \theta_{calc_j}(\mathbf{x})\right]^2}{\sigma_j^2}\right\}, \qquad (4)$$

with $\mathbf{x}$ – the position of the source, T_{obs_i} and T_{calc_i} – the arrival times observed and calculated from observation, θ_{obs_i} and θ_{calc_i} are the polarisation angles observed and

calculated, σ_i and σ_j are the uncertainties, and k is a normalisation constant.

The quality of the solution is assessed according to Lomax's recommendation (Lomax *et al.*[2009]). We consider the maximum likelihood hypocenter, defined as the point in space of the maximum value of the location *pdf* (Lomax and Snieder[1995]) and the corresponding origin time. The maximum likelihood (or minimum misfit) point of the complete, non-linear location *pdf*, is selected as an "optimal" hypocentre. The significance and uncertainty of this maximum likelihood hypocentre cannot be assessed independently of the complete solution *pdf*.

A relative measure of the volume of the high likelihood region of the location *pdf*, V_{pdf}, is given by:

$$V_{pdf} = \int_M \frac{pdf(\mathbf{x})}{pdf^{\max}} dV \quad , \tag{5}$$

where $pdf^{\max}$ is the maximum value of the location *pdf* in $\mathbf{M}$. The V_{pdf} is a measure of the "extent", if the V_{pdf} value is big the pdf tops up the volume. If the *pdf* is constant everywhere, the V_{pdf} is equal to the volume of the model space.

The advantage of this measure is the handiness to implement it in the Oct-tree algorithm.

We also examined statistics related to the solutions using the half-lengths of three principal axes of a 68% confidence error ellipsoid approximation to the location *pdf*. It is an ellipsoidal, "Gaussian" or normal statistic approximation to the *pdf*, truncated at the 68% confidence level. This confidence ellipsoid is generated from the covariance matrix $\mathbf{C}$ of the *pdf* scatter sample (Press *et al.*[1992]).

If the *pdf* was perfectly ellipsoidal, then there would be 68% probability that the hypocenter is inside the ellipsoid and the ellipsoid is centred on the maximum likelihood hypocenter. In fact, the maximum likelihood hypocenter can be outside of the ellipsoid – this is common with complicated or irregular (non-ellipsoidal) *pdf* shapes (Lomax *et al.*[2000]).

Anyway, it is well known that the Gaussian estimators and resulting confidence ellipsoid can be good indicators of the uncertainties in the location only in the case where the complete non-linear *pdf* has a single maximum and has an ellipsoidal form.

In addition, the location uncertainty can be non-ellipsoidal (non-Gaussian) because the forward calculation involves a non-linear relationship between hypocentre location and travel times (Lomax *et al.*[2001]).

Finally, another essential aspect for such location algorithms is the theoretical seismic wave travel-time dataset through a predefined velocity model enabling travel path calculations between any considered seismic source and receiver locations to determine the travel-time field, ray and paths take-off angles. There are three basic classes of methods to calculate travel-times and rays (full-waveform methods, ray methods, and eikonal and shortest-path, graph-based methods), among these the Fast-Marching Method (FMM) is chosen and used.

FMM solves the wavefront propagation problem through numerical solution of the eikonal equation for ray propagation, with repeated application of Huygen's principle while taking into account causality, that is to say that information only flows forward in time (Sethian[1999]). This condition makes the method unconditionally stable in the presence of shadow zones, diffractions, etc., and also makes it applicable to 2D and 3D regular and irregular grids, such as complex 3D velocity model, including significant mining voids or paste backfill zones.

In addition, the FMM also permits through post-processing of the travel-time field using finite-differences to follow the local time gradient back from the receiver to the source. This is of great importance for improving microseismic locations when using only a small number of sensors.

To make the location program efficient for complicated 3-D models, the travel times between each station and all nodes of an x, y, and z spatial grid are calculated once and then stored on disk as travel time grid files. The forward calculation during location reduces to retrieving the travel times from the grid files and forming the misfit function.

NUMERICAL TESTS

Synthetic Data

The localisation module implemented in SYTMISauto software used in this study, is based on the combination of the microseismic wave arrival times as well as the polarisation angles, in order to determine the hypocenter with the maximum likelihood.

Various numerical simulations were run to examine the robustness of the source location algorithm described above. Here, one of those numerical simulations is presented and it is carried out to assess the presence of an important mining void underlying a rather contrasted geological overburden made of different horizontal rock strata with different geophysical properties.

This illustrative numerical test is drawn from the field situation of Cerville-Buissoncourt cavern collapse experiment during which induced seismicity of thousand events was recorded by a high resolution near filed array (Contrucci *et al.*[2011]). In this case, both the modelled brine cavern and the overlying lithology have dimensions of the same order of amplitude to the distance and extension of the nearby microseismic array overlying the salt mine, approximately 120 meters for the cavern diameter,

125 meters for the geological overburden and 200 meters for the surface and subsurface microseismic array.

Two virtual hypocenters are positioned in the immediate vicinity of the 3D cavern, blocked and then localised (Figure 1) to compute theoretical arrival times, ray paths and take-off angles on 3D receivers.

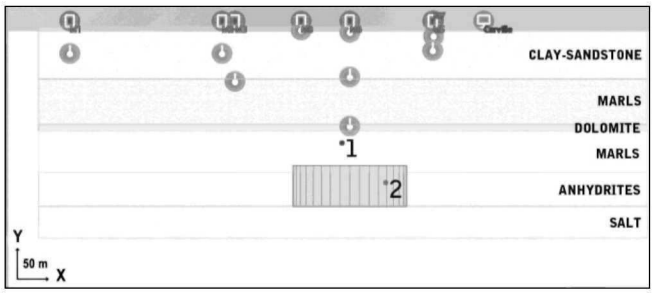

Figure 1: Section showing the two dots (1, 2) as the hypothetical sources with known positions. The cavern is modeled by a 150 m x 50 m cylinder and the big grey spheres illustrate the seismic array

Take-off angles are expected to constrain efficiently any direct search event location method since the seismic monitoring array offer a good coverage in *X* and *Y* but not in *Z* (depth). The first event is positioned just above the cavity, in the cap rock, the second besides the cavity, in the salt rock.

These two positions are representative of the two main mechanisms to be detected within the real seismic swarm to be processed, i.e. upward progression of the cavity along with the failure of the low strength cap rock and lateral extension of the cavity in the salt. The input data, i.e. computed travel times and polarization angles, are then disturbed assuming data errors associated to sources of inadequacies and uncertainties. We perturbed the polarization angles introducing gradually an error from 5 to 15° and the P-wave pickings introducing an error range from 0.001 to 0.10 s.

The two events are then localised twice, using a 3D velocity model first with the presence of the 3D cavern and second without it. The known geometry of the cavern was approximated by a 150 m × 50 m cylinder (Figure 1).

The misfits (x, y and z) between initial theoretical coordinates and the back calculated ones are showed in the Table I.

The results show clearly that the *x* and *y* coordinates are significantly influenced by the presence or not of a large void in the velocity model, and also the calculated depth changes drastically for the source prepositioned on the sidewall of the cavity. The cause is the very different ray paths computed in the case a 3D velocity model with or without cavity. An example of ray path computed with taking into account the mining void and the clustering of the *pdf* points are showed in the Figure 2.

Table I The misfits (mis.) indicate the differences between theoretical and calculated coordinates of the two hypothetical sources with known positions

	Mis. X (m)	Mis. Y (m)	Mis Z (m)	Mis. X (m)	Mis. Y (m)	Mis. Z (m)
	1. At the top, in the cap rock			2. On the side, in the salt rock		
Cavern	0	-2.45	-7.80	5.00	7.55	19.51
No cavern	0	-2.45	-7.80	-17.5	-14.95	14.53

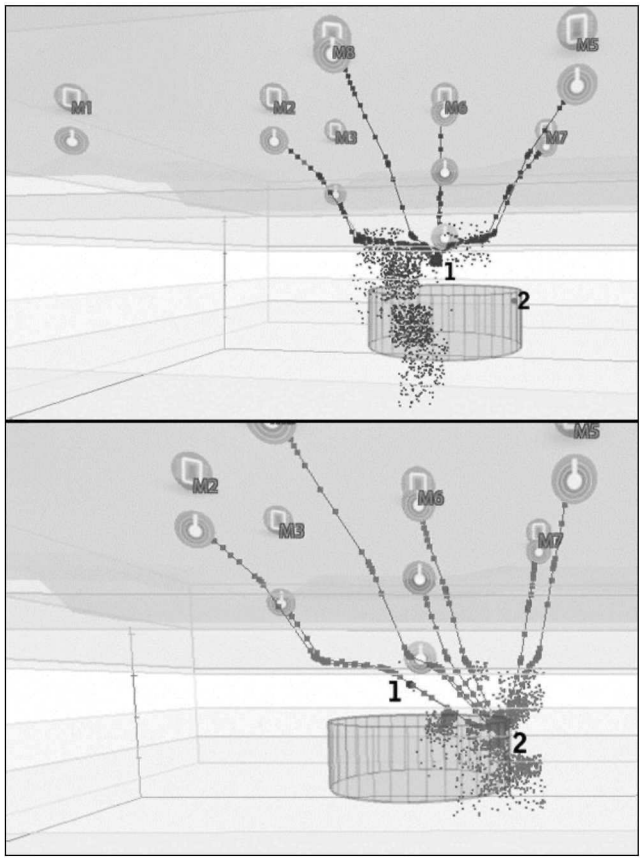

Figure 2. The ray paths and the probability density of the event location are shown for the two sources re-localised with taking into account the cavern in the 3D velocity model

In both cases the clusters of dots (Figure 2) are located around the points of the location and they are scattered, this is probably caused by the uncertainty in the spatial location due to the travel time calculation errors, velocity model, network geometry etc.

The quality of the determination of the hypocenters can be quantified and analysed using the high likelihood region of the location *pdf* and the half-lengths of the principal axes of a 68% confidence error ellipsoid fitting coarsely this volume (Table II). The pertinence of this last measure may be cautiously assessed through graphical representation, in fact to represent most completely the results of probabilistic, direct, global-search methodologies we used above all the geometrical properties of the location *pdf* .

Table II Example of the half-lengths of three principal axes of error ellipsoid. Axes 1, 2 and 3 are semi-major (longest), the semi-intermediate and semi-minor (shortest) axes, respectively, of the confidence ellipsoid

	Error Ellipsoid		
	Axis 1 (m)	Axis 2 (m)	Axis 3 (m)
Cavern	69.35	37.28	36.98
No cavern	93.52	43.84	35.02

Generally, the near-ellipsoidal form of the location *pdf* shows a well constrained location, and it is true for this numerical simulation for both locations (see Figure 3).

In the present case, the main difference is for the first axis (1) of the ellipsoid, which fits the z axis. As expected, the most sensitive component to the strong perturbation introduced through the cavern full of brine is the vertical coordinate.

GEOLOGICAL SETTING AND MINING PROCESS

For the next step validation of the 3D source location algorithm, based a true dataset, we chose a mine induced microseismic swarm issued from the same site described here before.

The geological setting is made of different sub-horizontal rock strata part of the eastern edge of the Parisian sedimentary basin, with:

- A first 120 meters thick overburden made of two distinguishable clay-sandstone-marl layers, with P-waves velocities are $V_{P1} \approx 3460$ m/s, $V_{P2} \approx 2500$ m/s.
- A 9 meter thick, very stiff, competent layer of dolomite and anhydrites, called the "Beaumont Dolomite" strata, characterized by a 2.9 KN/m^3 density, a UCS close to 200 MPa and a velocity V_{P3} estimated to 4660 m/s.
- A 55 meters thick strata of marls intertwined with indurated anhydrites ($V_{P4} = 3970$ m/s, $V_{P5} \approx 4620$ m/s).
- The salt deposit (V_{P6} estimated to 4030 m/s), lying between 185 to 340 meters deep.

From the feedback experience, the Beaumont dolomite layer plays a strong role in the overall stability of the overburden during the progressive enlargement of the brine field (Laouafa *et al.*[2012]). It qualitatively fulfils the function of a stiff elastic brittle frame able to support high stresses with low deformations before brutal failure (Nothnagel[2003]). Nowadays, this collapse is looked for by the miners in order to prevent any post-mining risk in the long-term future. This stratum is usually seen as a clear physical barrier separating two geological horizons, the underlying large salt deposit and its cap rock and the overlying geological burden. The seismic fracturing and goaffing process (generally associated to the longwall mining operation) of the 55 meters of cap rock may be considered then as a first critical stage of enlargement of the solution cavern. The following stage is supposed to be the progressive uncovering of the Beaumont Dolomite strata, showing a very weak, difficult-to-detect elastic response to most monitoring surface and subsurface sensors. Once the brine cavern reaches a second critical size, the Beaumont Dolomite rock strata is expected to fail brutally, leading straight to the catastrophic collapse up to the surface.

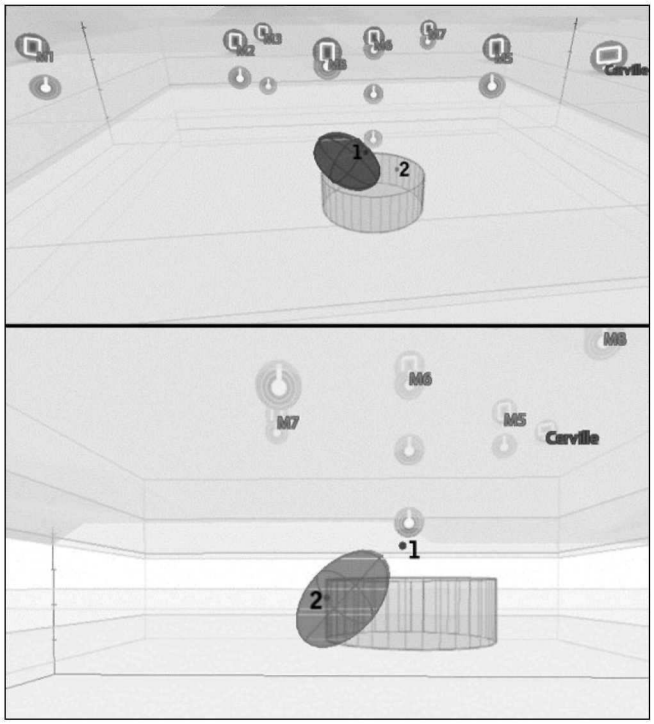

Figure 3. The error ellipsoid for the two sources re-localised with taking into account the cavern in the 3D velocity model

In 2007, the geometry of the brine cavern was surveyed by three dimensional sonar measurements. Seismic activity was almost inexistent. In March 2008, a microseismic crisis occurred, more than 10 000 events recorded in a few days (Contrucci *et al.*[2011]).

Although there was no doubt that this microseismicity was associated to the failure of the cap rock the question raised how much of it has failed and whether or not the first phase was eventually achieved.

Fortunately, the geometry of the brine cavern was surveyed by three dimensional sonar measurements once more. This revealed that 35 meters thick by 200 meters long of cap rock strata has failed, quite asymmetrically on the east part, with the fresh top of the cavern almost licking at the Beaumont Dolomite strata. Of course, all this information may be used as a dataset for the calibration of a 3D location procedure in a complex mining environment. This means a heterogeneous rock medium hosting a large and fast changing mining void and a critical need for

accurate location of the microseismic pattern to detect the entry into the last phase of development before large scale failure.

Forty microseismic events from the early stage of this seismic crisis and featuring clear easy-to-pick arrival times and polarised signals from the three components probes were selected to test and optimize the location procedure based on a 3D velocity model. Since this subset is selected on the early stage of the crisis, those events are reasonably thought to be located in the first ten meters above a non planar roof, located at an average elevation of a few meters inside the cap rock from the 3D survey.

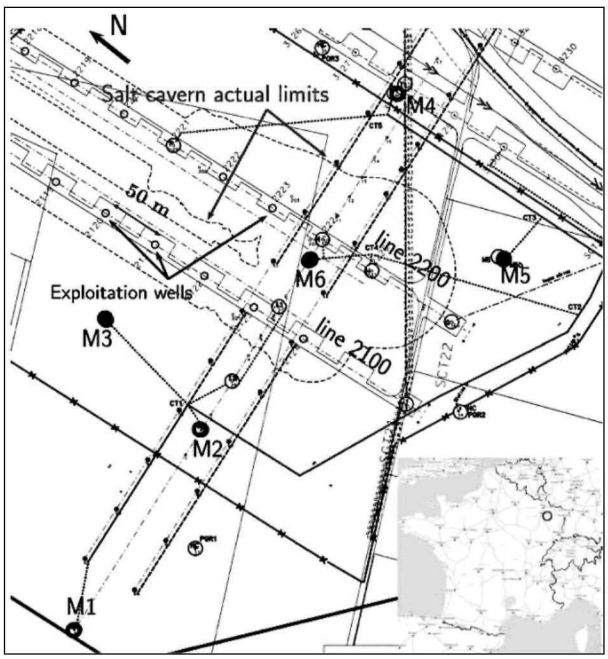

Figure 4. Plan view of the instrumented site of Cerville-Buissoncourt showing microseismic stations M1 – M6, the exploitation wells of line 2 100 and line 2 200, and the actual cavern limits (dashed line, from Mercerat *et al.*[2010])

The location of those events was first computed based on arrival times and emergent angles minimizing the misfit with the L-2 norm. As regards the Cerville-Buissoncourt experiment, the orientation of the 3-D probes installed in boreholes was measured with a retrievable attitude device before grouting.

Simulations were run to test the differences between the two locations (with or without cavity into the 3D velocity model); a first localisation was done without taking into account the cavern. The results were not completely satisfying (Figure 5), because the majority of the sources are located below the cavity in the salt formation, and this does not agree with the knowledge of roof cavern evolution. The gamma ray well-logging show that massive marls roof falls of ~500 000 m^3, i.e. 4.6 Mt of material, occurred between February and May 2008 with a transverse asymmetric roof elevation (Klein *et al.*[2008]), thus the majority of the sources would be located in the marl with more or less indurated anhydrites. These results lead to improve the input data for source location and above all the velocity model.

Thus, the next location of these 40 events was carried out with taking into account the cavern in the 3D velocity model (Figure 6). The results are quite different from the previous. This 3D location is characterized by few events located into the cavern and the others get on towards the dolomite layer and lie into the marl with anhydrite layer. There is also a strange concentration of sources around the M 6.3 geophone (last sensor above the cylinder), which was not used to localize the sources.

Nine events are located into the clay-sandstone-marl. No events of 2008 crisis are located into the dolomite layer. In addition, three events have an aberrant location, below the cavity.

Anyway, it could be plausible that there are microseismic sources into the cavern due to insoluble blocks which fall into the brine and seismic sources into the marls with anhydrite located inside the brine, due to the roof fall.

The study area is characterized by a kind of evolution of the microseismicity that migrates in space and time and this clearly indicates a generally vertical development of the cavern dome along with an apparent lateral dissymmetry.

Concerning statistics related to the two location solutions, there is no compact location *pdf* in both source locations, as show in the figures 5 and 6; this irregular *pdf* shape is probably due to the velocity model inaccuracy (Lomax *et al.*[2009]).

Another possible reason of the uncertainty source can be the absence of discontinuities in our velocity model, we introduced the different velocity values using a velocity gradient there is not a physical surface which distinguishes two different geological layers.

The ratio between the maximum axis and minimum axis of a 68% confidence error ellipsoid is always major than 1.5 (Figure 7), this determines an elongated error ellipsoid. This kind of ellipsoid highlights that the depth variation probability density is more relevant than lateral variation one and indicates above all no depth constraint (Lomax *et al.*[2009]). Reducing the vertical extent of the *pdf* requires stations at distances of the order of the source depth or less. The addition of one or more good quality S readings, especially at the closest stations, would further improve the depth constraint (Lomax *et al.*[2009]).

The ellipsoid volume values are quite comparable (Figure 8). The mean difference between ellipsoid volume of 3D velocity model with cavern and without cavern is 133.54 m^3.

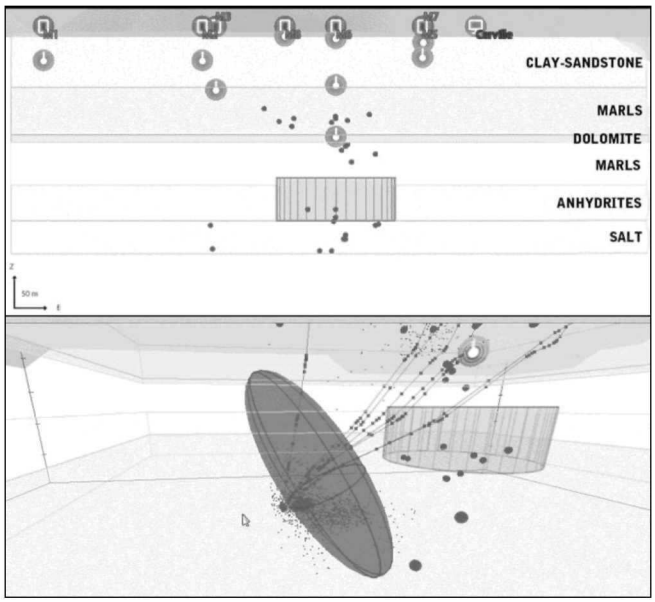

Figure 5. The XY view of microseismic event location (3D velocity model without taking into account the mining void). Below an example of ray path and error ellipsoid (the small grey dots represent the probability density of the event location)

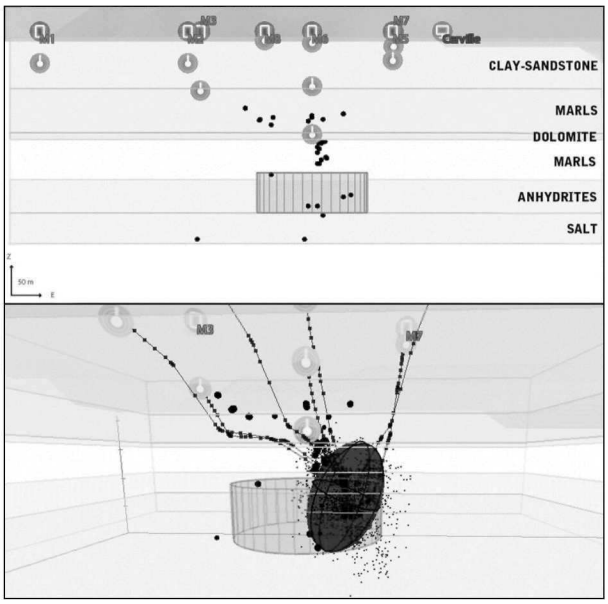

Figure 6. The XY view of microseismic event location (3D velocity model with taking into account the mining void). Below an example of ray path and error ellipsoid (the small black dots represent the probability density of the event location)

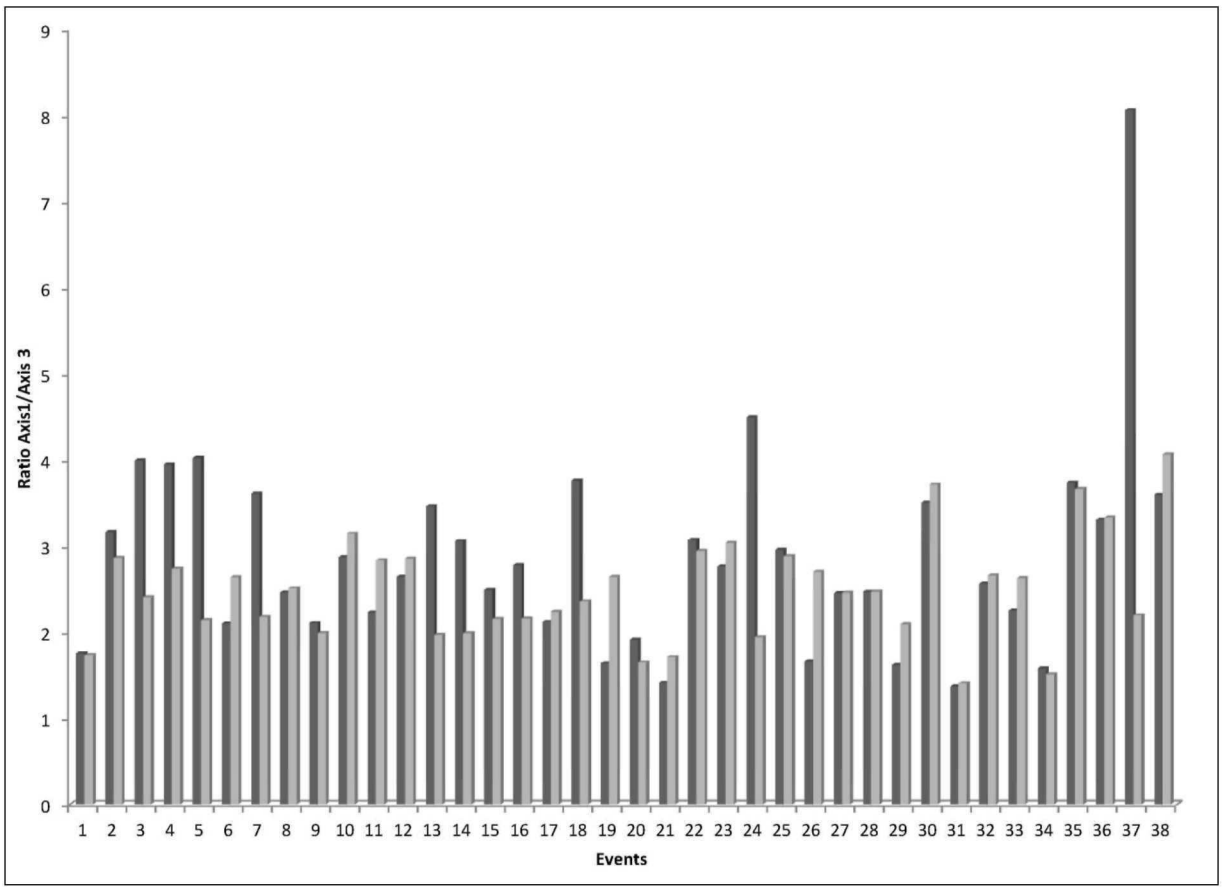

Figure 7. The ratio between the maximum axis (Axes 1) and minimum axis (Axes 3) of a 68% confidence error ellipsoid versus the number of events is presented. In light grey the values obtained with a 3D velocity model with cavity, in dark grey without cavity

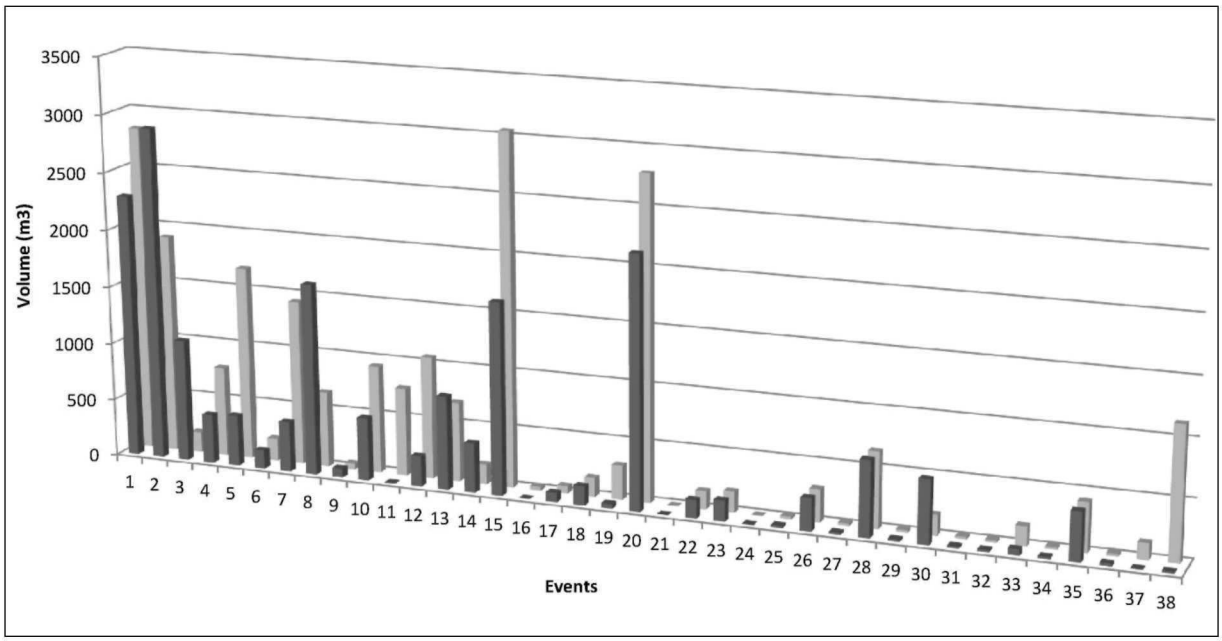

Figure 8. The high likelihood region of the location *pdf*, V_{pdf} , for the real events versus the number of events is presented. In light grey the values obtained with a 3D velocity model with cavity, in dark grey without cavity

However, in both locations (with or without mining void in the velocity model) the weighted, root-mean square of the arrival residual (observed-calculated) times, rms, is quite small and reasonable. So, this parameter without other information is not reliable to estimate the quality of a source location.

Clearly, all these results show that there are some aspects to improve, above all related to methodology and the specific Cerville site setting. The first is to introduce into the 3D velocity model the presence of interfaces among the different geological layers. Until now the different velocity values are introduced as a kind of velocity gradient without any physical separation, i.e. between the first layer and the second layer, etc. This lack probably influences significantly the travel time paths and consequently the final results. On the contrary, for traditional 1D velocity model we used defined interfaces to identify each geological layer.

Concerning the location methodology it will be also necessary to modify the assessment of statistics related to the solutions, the use of the half-lengths of three principal axes of a 68% confidence error ellipsoid is not sufficient; it indicates largely uncertain location of the hypocenter. It could be useful to adopt a classical confidence error ellipsoid with a 90% confidence error.

Finally, regarding Cerville site setting it is necessary to find a number of sources with a good quality of polarisation angles (the database with only about 40 events with polarisation angles is very small to give for the moment an exhaustive explanation of the source migration). Then, it could be interesting to improve again the velocity model, which is not a static model but evolves every time contemporary to the natural roof evolution by marl degradation in contact with the saturated brine. The 3D velocity model used derives from numerical simulation, which probably needs some new deep analysis of input parameters.

Moreover, the parameterization of the 3D V_p and V_s model is not based on average station spacing, the grid spacing of 5 m × 5 m × 3 m is adopted and this probably fits well with the microseismic source resolution above all in depth, but it is not adequate for the network geometry.

Nevertheless, the Cerville site is only a chance to test our algorithm.

DISCUSSIONS AND CONCLUSIONS

Nowadays, it is generally accepted that in mining environment the traditional monitoring methods cannot meet the needs of situation. In fact, the microseismic local network is considered one of the best tools to monitor.

In parallel, one effective way to improve location accuracy is to install more high resolution sensors, that is, to increase the sensitivity of the system so that more data are included in the location. Since the seismic system becomes more sensitive, it records many more events than before, which places a larger load on seismic processing staff. So, automatic source location become a fundamental aspect for mining management, but before passing to this step it is necessary to improve the source location algorithm.

Our aim is to obtain an absolute location, for microseismicity early-warning in mines, performed rapidly and in an evolutionary manner starting with the first available phase arrivals and polarization angles. An

automatic and accurate source location algorithm, which gives robust and useful location information, leaves more time for seismic staff for interpretation, hazard assessment, and risk management.

The first tests to apply our source location algorithm were done using numerical simulation and then with some real data coming from the Cerville salt cavern. Based on these results, the algorithm seems to work, but as expected, our first real database is not a perfect database to study the general microseismicity of the area (it is only a part of the main crisis of spring 2008). Moreover, in this instability mechanism the inertial effect may be significant as the roughness evolution during sliding, brine infiltration and dynamical crack propagation (Laouafa *et al.*[2012]), thus the processing of small magnitude events recorded locally calls for some precautions due to some near-field conditions adverse to accuracy.

However, the gain of the 3D location (much better separation of the fracturing processes in the cap rock and on the sidewalls of the cavern, discerning unambiguously the impact of the roof falls at the bottom of the cavity) starts to be achieved and other improvements in the 3D velocity model could lead to new satisfying goals.

In addition, it is necessary to test this source location algorithm with another case of study, for instance with a rich database coming from a deep mine, this could help us to validate in a complete and evolutionary way our 3D algorithm.

Anyway, this source location algorithm is currently being improved and automated for operational implementation in a deep mine.

ACKNOWLEDGMENTS

The authors would like to thank:

- SOLVAY, S.A. for the experimental site, the technical support and the data for site characterization.
- The European Commission for their support and the partners of the EU FP7 project I2Mine (http://www.i2mine.eu).
- RaSiM Organizing Committee and the reviewers for their comments that help to improve the manuscript.

Special thanks also go to Anthony Lomax for his advice, counsel and expertise about the localisation methodology.

REFERENCES

CONTRUCCI, I., KLEIN, E., CAO, N.-T., DAUPLEY, X. and BIGARRE, P. Multi-parameter monitoring of a solution mining cavern collapse: First insight of precursors, *Comptes Rendus Geoscience*, vol. 343(1), 2011. pp. 1–10.

GIBOWICZ, S.J. and KIJKO, A. *An introduction to mining seismology*, Academic Press, San Diego, 1993. 399 p.

HANDLEY, M. Improved locations of mine seismic events, *Feature innovative*, vol. 1, 2006. pp. 34–35.

HUDYMA, M. and POTVIN, Y. An engineering approach to seismic risk management in hardrock mines, *J. Rock Mech. and Rock Eng.*, vol. 43, 2010. pp. 891–906.

HUSEN, S., KISSLING, E., DEICHMANN, N., WIEMER, S., GIARDINI, D. and BAER, M. Probabilistic earthquake location in complex three-dimensional velocity models: Application to Switzerland, *J. Geophys. Res.*, vol. 108(B2), 2003.

IANNACCHIONE, A.T., MARSHALL, T.E., BURKE, L., MELVILLE, R. and LITSENBERGER, J. Safer mine layouts for underground stone mines subjected to excessive levels of horizontal stress, *Min. Eng.*, vol. 4, 2003. pp. 25–31.

KLEIN, E., CONTRUCCI, I., DAUPLEY, X., HERNANDEZ, O., BIGARRE, P., NADIM, C. and CAUVIN, L. Experimental monitoring of a solution-mining Cavern in Salt: identifying and analyzing early-warning signals prior to collapse, in *Proc. SMRI Tech. Conf.*, Texas, USA, 2008. pp. 135–146.

LIPPITSCH, R., WHITE, R. and SOOSALU, H. Precise hypocentre relocation of microearthquakes in a high-temperature geothermal field: The Torfajokull central volcano, Iceland, *Geophys. J. Int.*, vol. 160, 2005. pp. 370–387.

LOMAX, A. and SNIEDER, R. Identifying sets of acceptable solutions to non-linear, geophysical inverse problems which have complicated misfit functions, *Nonlinear Processes in Geophys.*, vol. 2(3/4), 1995. pp. 222–227.

LOMAX, A., VIRIEUX, J., VOLANT, P. and BERGE, C. Probabilistic earthquake location in 3D and layered models: Introduction of a Metropolis-Gibbs method and comparison with linear locations, in *Advances in Seismic Event Location* (eds. Thurber, C.H. and Rabinowitz, N.), Kluwer, Amsterdam, 2000. pp. 101–134.

LOMAX, A. and CURTIS, A. Fast probabilistic earthquake location in 3D models using oct-tree importance sampling, *Geophys. Res. Abs.*, vol. 3, 2001. p. 955 (www.alomax.net/nlloc/octtree).

LOMAX, A., ZOLLO, A., CAPUANO, P. and VIRIEUX, J. Precise absolute earthquake location under Somma-Vesuvius volcano using a new 3D velocity model, *Geophys. J. Int.*, vol. 146, 2001. pp. 313–331.

LOMAX, A. A reanalysis of the hypocentral location and related observations for the Great 1906 California Earthquake, *Bull. Seism. Soc. Am.*, vol. 91, 2005. pp. 861–877.

LOMAX, A., MICHELINI, A. and CURTIS, A. Earthquake location, direct global-search methods,

in *Encyclopedia of complexity and system science* (Part 5), Springer, New York, 2009. pp. 2449–2473.

LAOUAFA, F., CONTRUCCI, I. and DAUPLEY, X. In-situ large monitoring and numerical modeling of the loss of stability of salt cavity, in *Mechanical Behaviour of Salt VII* (eds. Bérest, P., Ghoreychi, M., Hadj-Hassen, F. and Tijani, M.), Taylor and Fransis group, London, 2012. pp. 171–178.

MENDECKI, A.J. *Seismic monitoring in mines*, Chapman and Hall, London, 1997. 275 p.

MERCERAT, E.D., DRIAD-LEBEAU, L., BERNARD, P. Induced seismicity monitoring of an underground salt cavern prone to collapse, *Pure Appl. Geophys.*, vol. 167, 2010. pp. 5–25.

NOTHNAGEL, R. *Modélisation des instabilités en Mécanique des Roches: application à l'exploitation de la concession de Drouville*, PhD Thesis, Ecole des Mines de Paris, France, 2003. 255 p. (in French).

PAVLIS, G.L. Appraising relative earthquake location errors, *Bull. Seism. Soc. Am.*, vol. 82, 1992. pp. 836–859.

POTVIN, Y. and HUDYMA, M.R. Keynote address: Seismic monitoring in highly mechanized hardrock mines in Canada and Australia, in *Proc. 5th Int. Symp. on Rockbursts and Seismicity in Mines: Dynamic Rock Mass Response to Mining* (eds. Van Aswegen, G., Durrheim, R.J. and Ortlepp, W.D.), Southern African Institute of Mining and Metallurgy, 2001. pp. 267–280.

PRESS, W.H., FLANNERY, B.P, SAUL, A.T. and VETTERLING, W.T. *Numerical recipes*, Cambridge University Press, New York, 1992.

PRESTI, D., TROISE, C. and NATALE, G.D. Probabilistic location of seismic sequences in heterogeneous media, *Bull. Seism. Soc. Am.*, vol. 94, 2004. pp. 2239–2253.

RICHARDS-DINGER, K.B. and SHEARER, P.M. Earthquake locations in southern California obtained using source-specific station terms, *J. Geoph. Res.*, vol. 105, 2000. pp. 10939–10960.

SETHIAN, J.A. *Level set methods and fast marching methods*, Cambridge University Press, Cambridge, 1999. 378 p.

SHEARER, P.M. Parallel fault strands at 9-km depth resolved on the Imperial Fault, Southern California, *Geoph. Res. Lett.*, vol. 29(14), 2002.

SPENCE, W. Relative epicenter determination using P-wave arrival time differences, *Bull. Seism. Soc. Am.*, vol. 70, 1980. pp. 171–183.

SPILLMANN, T., MAURER, H., GREEN, A.G., HEINCKE, B., WILLENBERG, H. and HUSEN, S. Microseismic investigation of an unstable mountain slope in the Swiss Alps, *J. Geophys. Res.*, vol. 112, 2007.

SUFFERT, J., GRANDJEAN, G. and BITRI, A. Étude d'une cavité saline par méthodes sismiques, *Rap. De Stage*, 2006 (in French).

TARANTOLA, A. and VALETTE, B. Inverse problems = quest for information, *J. Geoph. Res.*, vol. 50, 1982. pp. 159–170.

WALDHAUSER, F. and ELLSWORTH, W.L. A double-difference earthquake location algorithm: Method and application to the northern Hayward fault, California, *Bull. Seism. Soc. Am.*, vol. 90, 2000. pp. 1353–1368.

WALDHAUSER, F. and ELLSWORTH, W.L. Fault structure and mechanics of the Hayward Fault, California, from double-difference earthquake locations, *J. Geophys. Res.*, vol. 107(B3), 2002.

ZEMBATY, Z. Mine induced rockbursts – ground motion analysis, in *Proc. 11th Int. Conf. on Soil Dynamics and Earthquake Eng., Proc. 3rd Int. Conf. on Earthquake Geotech. Eng.*, Berkeley, USA, vol. 1, 2004. pp. 228–234.

ZOLLO, A., MARZOCCHI, W., CAPUANO, P., LOMAX, A. and IANNACCONE, G. Space and time behavior of seismic activity at Mt. Vesuvius Volcano Southern Italy, *Bull. Seism. Soc. Am.*, vol. 92, 2002. pp. 625–640.